Chemical Engineering Journal 284 (2016) 657–667

Contents lists available at ScienceDirect

Chemical Engineering Journal

journal homepage: www.elsevier.com/locate/cej

Bulk processing of ZnO nanostructures *via* microwave assisted oxidation of mechanically seeded Zn dust for functional paints and coatings

Santhosh Balanand [a], Mathews Jeen Maria [a], T.P.D. Rajan [b], A. Peer Mohamed [a], S. Ananthakumar [a,*]

[a] *Functional Materials Section, Materials Science and Technology Division, CSIR-National Institute for Interdisciplinary Science and Technology, Thiruvananthapuram, Kerala 695 019, India*

[b] *Minerals and Metallic Materials Section, Materials Science and Technology Division, CSIR-National Institute for Interdisciplinary Science and Technology, Thiruvananthapuram, Kerala 695 019, India*

HIGHLIGHTS

- Bulk ZnO nanostructures from Zn dust via microwave oxidation, a catalyst-free/rapid technique.
- Mechanically activated ZnO seed layer, accelerating oxidation kinetics.
- Functional paints and coatings developed with nano ZnO + CNSL resin.
- Coatings validated for IR shielding and corrosion resistance applications.

GRAPHICAL ABSTRACT

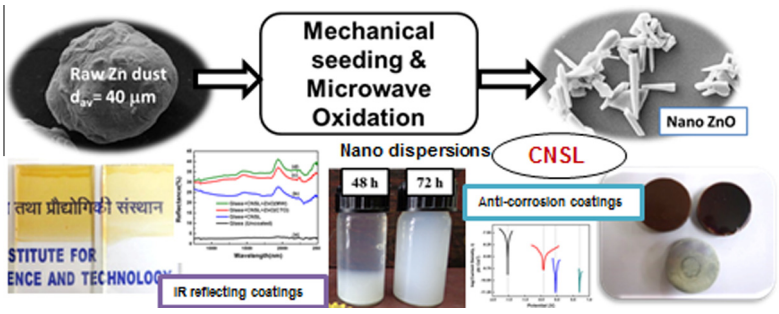

ARTICLE INFO

Article history:
Received 20 May 2015
Received in revised form 24 August 2015
Accepted 31 August 2015
Available online 11 September 2015

Keywords:
Zn dust
Mechanical seeding
Microwave oxidation
Nano ZnO
NIR-reflectance
Corrosion resistance

ABSTRACT

Micron sized metallic zinc dust (99.9%, D_{avg} = 40 μm) was mechanically milled to have zinc oxide seed nuclei on its surface, eventually transforming it into ZnO nanostructures by microwave irradiation for 15 min. Effect of milling on the growth of seed layer, oxidation kinetics, particle size distribution, nano ZnO morphologies, phase purity, dispersion and UV absorption properties were studied and reported. ZnO rods with length 5–6 μm and diameter of nearly 200 nm were successfully synthesized in bulk through this facile route. The products were systematically characterized and studied with the motive to design multifunctional nano-products. A paint formulation was made by blending the as-synthesized nano ZnO with a natural organic resin; *cashew nut shell liquid* (CNSL) and surface coatings were developed over glass and metal substrates. ZnO–CNSL paint coatings were further studied for NIR reflectance, optical transparency and hydrophobic surface property. Its effective corrosion resistance has been validated with highly corrosive Mg-alloy substrates, an upcoming key material for automobiles. The ZnO–CNSL paint developed showed about 33% enhancement in NIR shielding and about 156% improvement in corrosion resistance when compared to their uncoated counterparts. The study strongly recommends microwave accelerated oxidation as a technologically competent process for the bulk preparation of multifunctional nano ZnO.

1. Introduction

Metallic Zinc (Zn) and Zinc oxide (ZnO) have great industrial relevance owing to their inherent multi-functional properties [1–5]. Zn is a hexagonally close packed [6] and dense material

* Corresponding author.
E-mail address: ananthakumar70@gmail.com (S. Ananthakumar).

http://dx.doi.org/10.1016/j.cej.2015.08.163
1385-8947/

[7] widely used for automotive alloys [8], protective coatings [7,9,10], pigments [11] and even in water-splitting thermochemical reactions [12,13]. Similarly, ZnO due to its wide band gap (3.36 eV) coupled with high excitation binding energy (~60 meV) [5,14], is an attractive material for transparent conductors, sensors, functional cosmetics and catalysts [4]. Use of nano ZnO in surface coatings has endowed properties such as improved corrosion resistance [7,9], UV and IR shielding [15,16], antifouling [17], self-cleaning [18] and anti-icing [19] capabilities. At present, industrial demand for nano ZnO is steadily growing and many ZnO nanostructures such as nanorods, nanowires, nanobelts, nanotubes, nanotetrapods, nanocombs and nanocages [20,21] are being explored for diverse applications, specifically in nanoelectronic device fabrication. Meanwhile, various synthesis procedures like thermal evaporation [22,23], sol–gel [24], hydrothermal [25], mechano-chemical [26], sonochemical [27], etc. are well verged for nano ZnO production. However, new techniques for the economical production of nano ZnO with high product yield, speckled morphologies and enriched properties are still emerging. Maciel et al. [28] reported the synthesis of nano ZnO *via* thermal oxidation method, described it as a simple, low cost, low energy and catalyst free technique. Direct oxidation of Zn foils at different temperatures was studied by Yuan et al. [29] for developing varied ZnO morphologies in nano scale. In the work, Nano needles having diameters ranging from 80 nm to 20 nm (root to tip) were developed by direct oxidization of Zn foils at 500 °C. Though direct oxidation appears to be simple and clean, Zn–ZnO conversion by routine thermal treatment processes need extensive reaction time and high operational temperatures. Application of microwave heating is an impressive and rapid technique that can be exploited for the bulk production of nano ZnO [30].

Microwave at a frequency of 2.45 GHz develops volumetric heating through molecular interaction depending upon the dielectric nature of the material [30]. Use of microwave energy in solution chemistry for the nucleation and growth of nano scaled inorganic oxides are widely reported, but only for laboratory scale production [30]. Microwave-assisted synthesis has been described as an environment friendly approach for developing high quality nanostructures [30]. Zou et al. [31] adopted a microwave assisted hydrothermal method for synthesizing submicron (200–500 nm) Cu/Cu_2O nano-heterostructures with enhanced photodegradation efficiencies (92.1%) and improved absorption ratios. Wu and co-workers [32], successfully synthesized highly pure nano crystallites of SnO particles with size <30 nm using microwave assisted technique. The formation of mono-dispersed spherical ZnO in clusters (sizes from 274 nm to 50 nm) by a rapid microwave-polyol based process was reported by Hu et al. [33]. ZnO nanostructures with flower like morphology were attained without the aid of any ionic liquids or surfactants, using microwaves (irradiated for 10 min) was reported by Krishnakumar et al. [34]. Similarly, Phuruangrat et al. [35] prepared hexagonal nano flowers of ZnO having spear shaped nano rods in them with an aspect ratio in the range 40–80 by microwave irradiation (180 W/20 min) of the aqueous precursors. However, till date there are no reports on microwave aided direct thermal oxidation of micron sized Zn dust, which is addressed in this work.

Distinctive material modification *via* mechanical milling is profoundly discussed nowadays owing to its advantages like increased reactivity at lesser reaction time and with higher product yield and quality [36]. Ball milling process triggers surface oxidation on zinc metal, initiating an atomic scale seed layer formation which is a quite attractive initial modification procedure for the raw dust before the subsequent thermal oxidation steps [37].

In this work, direct thermal oxidation of ball milled Zn dust was conducted using a domestic microwave oven (at maximum power rating – 600 W, 2.45 Hz) and also a conventional muffle furnace for comparison. The NIR reflectance and anti-corrosion imparted by nano ZnO dispersed in a low cost organic natural resin (CNSL) were studied with the motive to develop low cost functional coatings for aforementioned applications. Thus, this work look forward to report a novel industrial scale-up route for nano ZnO synthesis from raw Zn dust resource which is simple, green, cost effective and energy efficient, with salient final functional potentials.

2. Experimental details

2.1. Raw material activation: milling of Zinc dust

Zn dust (99.9%) having particle size in the range 30–50 μm gifted by Binani Zinc Pvt. Ltd. was used as the source for the processing of bulk nano ZnO. Zn dust was charged into poly propylene containers along with ceramic milling-media and distilled water. Milling was employed for different time periods 12, 24, 48, 60 and 72 h in order to reduce the particle size. Typical milling conditions and process parameters chosen for the study are given in Table 1.

The milled Zn dust was again hand milled using mortar and pestle for a period of 15 min with graphite powder (10% by wt.). Graphitic Zn dust readily interacts with microwaves and generates volumetric heat at a faster rate [30,38].

The thermal conductivity of the reactant mixture is also improved, aiding the rapid heat absorption and thus reducing the reaction time for oxidation. Graphite will be burnt out during the heating process and will no way affect the final oxide formed [39].

2.2. Thermal oxidation of Zn dust

The thermal oxidation of the Zn dust was conducted *via* two routes; (i) Conventional thermal oxidation route (CTO) and (ii) Microwave assisted oxidation route (MW). In both the techniques, the milled Zn dust were spread into thin uniform bed of about ~2 mm thickness in a rectangular alumina boats of size 15 mm × 8 mm × 10 mm.

The crucible was loaded into a domestic Teflon-lined microwave cavity (Samsung; Power 1100 W and 2.45 GHz) for the microwave assisted oxidation besides into a closed muffle furnace for conventional oxidation. The maximum microwave power irradiated in pulse mode was 600 W, while in conventional heating; the power rating of the electrically operated muffle furnace was 7.5 kW. The whole milling and oxidation steps were randomly optimized. Table 2 shows the details of the oxidation conditions and constraints, the condition chosen for the final product synthesis is shown bold in the table.

Holding time and operating temperature were the two constraints chosen in the case of conventional oxidation technique whereas irradiation time and power in the case of microwave method. Zinc dust milled at regular time intervals *viz.* 24, 48, 72 h were used for the heat treatment in both the processing

Table 1
Ball milling parameters chosen for milling the raw Zn dust.

Vessel volume (cm^3)	250
Powder charged (g)	15
BPMR[a]	4.5:1
Zirconia Ball diameter (mm)	10
Milling medium (liquid carrier)	Distilled water
Milling atmosphere	Air
Rotar speed (rev/min)[b]	250
Milling time (h)	12–72

[a] BPMR– Ball to Powder Mass ratio.
[b] Rotar speed was measured using a Tachometer, in revolutions per minute (rev/min).

Table 2
Process details for conventional thermal oxidation (CTO) and microwave oxidation (MW).

Processing route	Processing conditions
	Milling time (h), Holding temperature (°C), Holding time (h)
Conventional thermal oxidation (CTO)	24,450,4
	24,600, 5.5
	24,750,7
	48,450,4
	48,600,5.5
	48,750,7
	72,450,4
	72,600,5.5
	72,750,7
	Milling time (h), Irradiation power (W), Irradiation time (min)
Microwave assisted oxidation (MW)	24,450,15
	24,600,10
	24,600,15
	48,450,15
	48,600,10
	48,600,15
	72,450,15
	72,600,10
	72,600,15

Values shown in bold are the optimal processing conditions chosen.

routes. The schematic of the final processing route is shown in Fig. 1.

2.3. Characterization of nano ZnO

The change in size and shape of micron sized Zn and the nature of particle fracturing due to milling was studied using Stereomicroscope (Leica DM 2500 P). The nano ZnO seed formation during milling was identified from the absorption spectra using UV–vis spectrophotometer (UV-2401 PC, Shimadzu, Japan), within the wavelength range of 200–800 nm. Thermo gravimetric analyses (TGA, Shimadzu TGA-50 Thermal Analyzer) of mechanically modified raw Zn dust were conducted in oxygen atmosphere from room temperature to a temperature of 700 °C at a heating rate of 10 °C min^{-1} to understand the advantage of milling operation in the conversion of Zn dust to nano ZnO. Powder X-ray Diffraction analysis (XRD, Philips X'pert pro PW 1710) was used to confirm the growth of ZnO seed nuclei with milling and for the final oxide formation. Crystallinity was measured within the angle range $2\theta = 20°–80°$. The lattice parameters of the ZnO formed was calculated from the XRD data using the equation [40]:

$$1/d^2 = 4/3[1/a^2] + [1/c^2] \quad (1)$$

where 'd' is the interplanar distance, 'a' and 'c' are the lattice parameters in nm (for hexagonal $c/a = (8/3)^{1/2}$). The nano crystallite size of the ZnO seeds and the final ZnO were also calculated from the XRD data, using Debye–Scherrer equation [40]:

$$D_{XRD} = (0.9\lambda)/(\beta\ Cos\theta) \quad (2)$$

where D_{XRD} refers to the average nano crystallite size in nm obtained from the calculation, 'λ' is the wavelength of the X-ray radiation in nm, 'β' is the full width at half maximum intensity measured in radian, and 'θ' is the diffraction angle in degrees. The average particle size (D_{avg}) distribution (Zeta-Size, Malvern Instrument, NANO ZS) of the ZnO seeds formed was also analyzed using dynamic light scattering (DLS) technique in water medium. The morphological features were perceived using Scanning Electron Microscopy (SEM, Zeiss, EV018) and Transmission Electron Microscopy (TEM, FEI Tecna 30G^2S – Twin Transmission). Selected area electron diffraction (SAED) patterns were also used for ascertaining the crystallinity of the samples.

2.4. Application study

The industrial applications of Zn dust derived ZnO was tested for multifunctional paint coatings with NIR reflectance and corrosion resistance. Cashew Nut Shell Liquid (CNSL, Vijayalaxmi Cashew company Pvt. Ltd., Kerala), a cheaply available organic base was selected as the paint medium. The synthesized nano ZnO (5 and 10 vol%) was dispersed in CNSL using mechanical stirrers and ultrasonication. The paint formulation obtained was coated

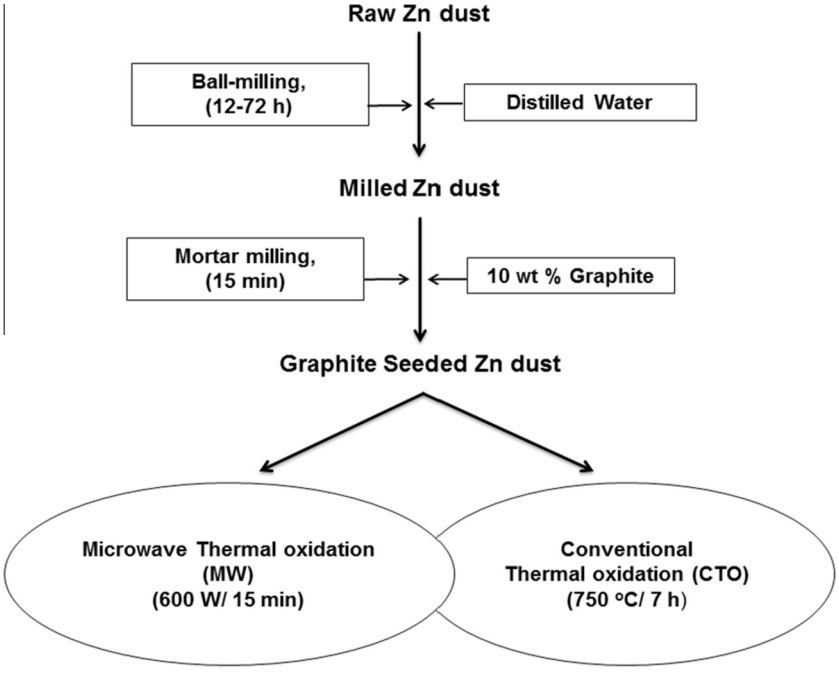

Fig. 1. Process scheme for the synthesis of nano ZnO.

on glass substrates using a computer controlled dip-coater (KSV instruments, Netherlands) and on AZ31 Mg alloy surface using brush. The Contact Angle (CA) measurement was done using a Tensiometer (Dataphysics-DCAT 11, Germany) *via* 'Wilhelmy balance method' to determine the wettability of the coating. The near infrared reflectance (NIR) spectra of the coatings were measured using UV–vis–NIR spectro-photometer (Shimadzu, UV-3600 with an integrating sphere attachment, ISR 3100) using Teflon (PTFE) as Ref. [41]. The IR data was recorded in the range from 700 to 2500 nm. The NIR solar reflectance (R^*) in the wavelength range from 700 to 2500 nm, which is the fraction of the incident solar radiation reflected by a surface, is the irradiance weighted average of its spectral reflectance, $r(\lambda)$, at the mentioned wavelength range. This can be calculated using the relationship (as per ASTM Standard E891-87) [41].

$$R^* = \int_{700}^{2500} (r(\lambda) \cdot i(\lambda) \cdot d(\lambda)) / \int_{700}^{2500} (i(\lambda) \cdot d(\lambda)) \quad (3)$$

where '$r(\lambda)$' is the experimentally obtained spectral reflectance (W m^{-2}) and '$i(\lambda)$' is the solar spectral irradiance (W m^{-2} nm^{-1}).

For corrosion testing, the as cast Mg alloy AZ31 was used. The specimens were machined to cylindrical blocks (4 mm D × 1 mm H). The face to be coated was polished with emery paper (#1600) and was cleaned and degreased using acetone and ethanol respectively. The corrosion test was conducted with (Electrochemical Analyser, CH instruments, Inc., Model no. 608E) 3.5% NaCl solution (salt water) as per standard guidelines in ASTM G5-94. The Corrosion potential (E_{corr}) and Corrosion current (I_{corr}) were measured using the instrument software. The corrosion was studied at ambient temperature conditions (27 °C) over a test surface area of 200 mm^2 with a test run period of 2400 s.

3. Results and discussions

3.1. Mechanical activation of Zn dust

Mechanical milling produces kinetically active reactant mixture with decreased particle size and defective lattice structure which can catalyze chemical transformations at low temperatures [35,42]. The mechanical operation is considered as an effective activation step to achieve direct oxidation of Zn dust at low temperatures. In the current study, the micron sized raw Zn dust was initially milled with the motive to reduce the particle size. Zinc is a low hardness (2.5 in Mohs scale) possessing metal having a HCP crystal structure with high axial ratio [c/a = 1.856]. The reduction in number of slip systems in the crystal results in shearing under the application of a mechanical force [43]. The effect of ball milling on the size, morphology and surface of the micron sized raw Zn dust at various stages of milling are shown in Fig. 2.

In Fig. 2a, the SEM image confirms that the as received raw Zn dust is a dense, spherical particle. Continuous milling induces sequential morphology changes in this inherently soft Zn particle. During milling, the Zn dust undergoes a ductile to brittle transition [43] causing the shearing and tearing of the particle leading to the powdering of Zn dust, which is evident from the SEM images (Fig. 2b–e). In Fig. 2b, the SEM image shows that 12 h of milling has produced physically elongated, flaky Zn discs clearly revealing the shearing which has taken place due to high impact energy. After 24 h of milling, these elongated Zn flake structurally collapse into weakly bonded fragments of size <5 μm. At this stage, the brittle fracture is clearly evident and the particle cleavage growth is more perceptible and wide spread (Fig. 2c). From Fig. 2d it can be observed that, 48 h of milling has caused further outspreading of the cleavage growth, resulting in the formation of a physically weak porous metal-frame work, indicating its readiness to get powdered within few hours of milling. It is evident from Fig. 2e that the fine powdered particles are having a physical size <2 μm after 72 h of milling.

The sequential break down of the metallic Zn dust during ball milling is further viewed at 24, 48 and 72 h of milling under optical microscope to validate the mechanism proposed. Fig. 3 shows the optical microscopic images of the Zn dust at various stages of milling.

Initially, the Zn dust shows extensive plastic deformation. Shearing and particle elongation is clearly seen at this stage. Later, a transition of polycrystalline Zn from ductile to brittle was observed. In hexagonally close packed crystalline Zn metal the basal cleavage cracks usually occurs at the (0001) plane [43]. Milling generates micro cracks during shearing due to high impact energy. Upon continuous shearing, the micro-cracks produce mechanically weak zones where the necking develops. The multiple cleavage cracks developed at different regions of the particle finally lead to metal fracturing. In addition to this accommodation mechanism other failure mechanisms like twinning, kinking and limited slips also induce metal cleavage and resulting fracture [43].

The aqueous milling of Zn dust produces ZnO seed nuclei due to the oxidation of surface Zn atoms. The ZnO seeding triggered by milling is evident from the UV–vis spectra of the milled Zn dust dispersion collected at different time intervals (*viz* 24, 48, 72 h). The UV analysis in Fig. 4a clearly gives the characteristic absorption peaks of ZnO in the UV region with maximum absorption in

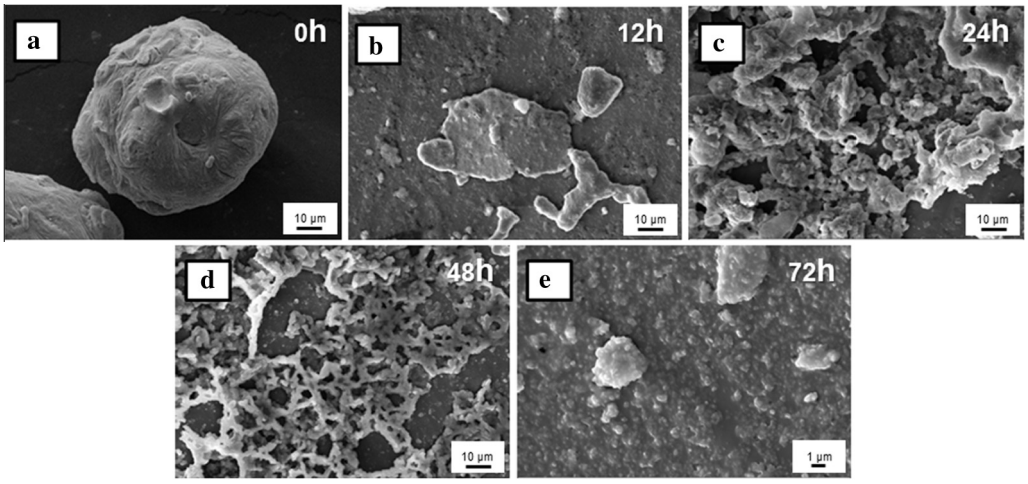

Fig. 2. SEM images of (a) un-milled raw Zn dust, (b) 12 h milled, (c) 24 h milled, (d) 48 h milled, (e) 72 h milled Zn dust.

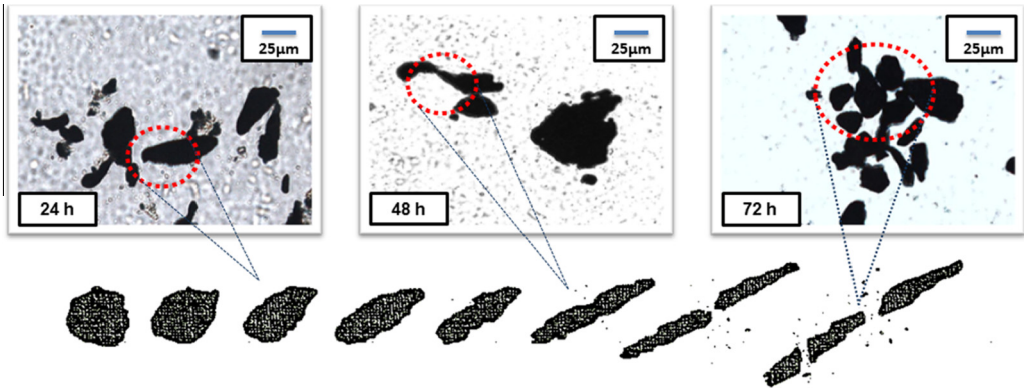

Fig. 3. Schematic illustration of the cleavage growth and particle fracturing occurring at different time intervals during milling (supported with optical images at different time intervals).

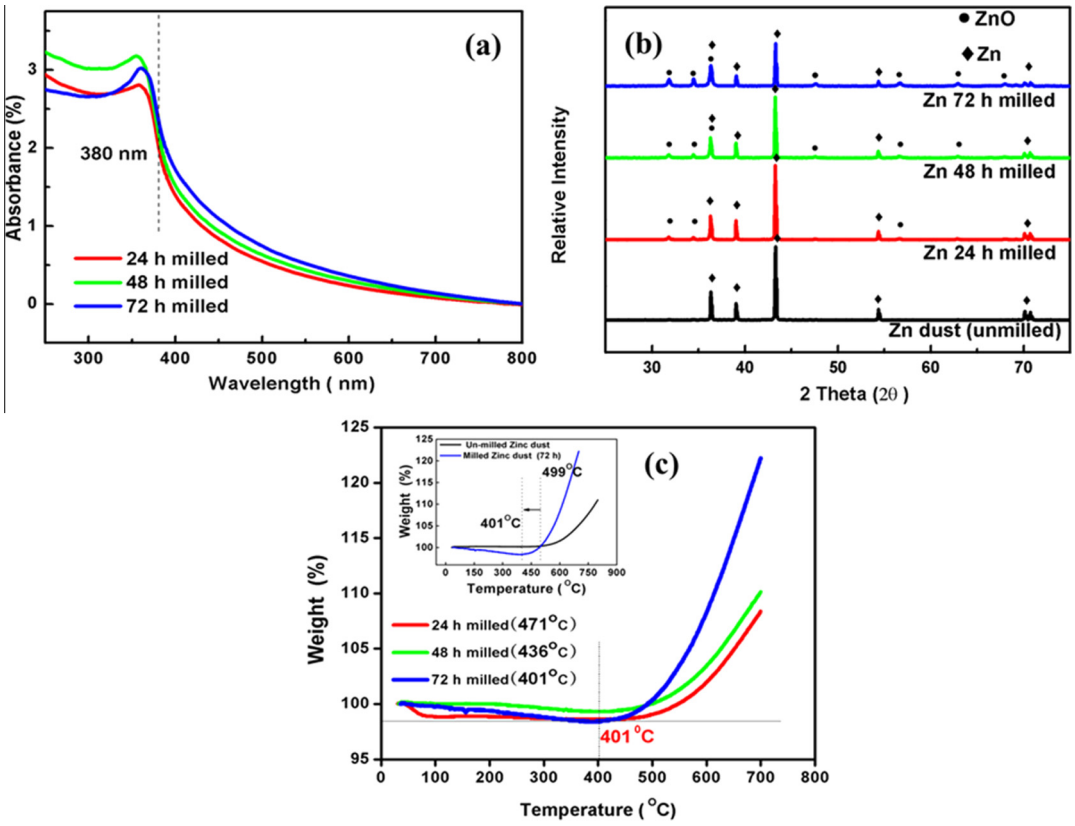

Fig. 4. (a) UV–vis spectrum, showing traces of ZnO in the milled and sonicated Zn dust. (b) XRD patterns of the Zn dust milled for different time intervals. (c) TGA of Zn dust in oxygen atmosphere (0–700 °C) (Inset shows drop in the oxidation onset temperature milled and un-milled Zn dust).

the wavelength range 360–370 nm, indicating the seeds grown during milling. The XRD results shown in Fig. 4b also confirms the ZnO seeding with the milling of Zn dust. The diffraction peaks obtained at the 2θ positions 36.28, 39.07, 43.33, 54.32, 70.35 and 70.72 corresponds to the lattice planes (002), (100), (101), (102), (103), and (110) of pure Zn metal (JCPDS PDF #00-004-0831). In the unmilled Zn dust these characteristic peaks were prominent while no traces of ZnO were observed. Milling this Zn dust for about 24 h, ensued the sprouting of ZnO peaks in the powder, the peaks obtained at positions 31.91, 34.45, 36.28, 47.60, 56.64, 62.82, and 67.93 corresponds to the (100), (002), (101), (102), (110), (103) and (112) lattice planes of wurtzite phase ZnO (JCPDS no: 36-1451). With increase in the milling time from 24 h to 48 h, these ZnO peaks became more apparent validating the claim of ZnO seeding. After about 72 h of milling, all the major peaks corresponding to ZnO became distinct and clear showing the ZnO seeding due to the faster growth of surface ZnO with milling. The progressive drop in the peak intensity of Zn with milling time is also a clear indication of the conversion happening with milling (Fig. 4b).

Zn dust in its pure form has a theoretical melting point at 419 °C and a boiling point of 908 °C. However, the aqueous milled Zn dust develops seeds of zinc oxy hydroxide on its surface. The TG analysis of the 24 h milled Zn dust showed a mild weight loss between 51 °C to 142 °C (Fig. 4c). It is probably due to the decomposition of these $Zn(OH)_2$ formed as a result of the hydrolysis reaction. The Zn $(OH)_2$ formation is earlier reported to have very low decomposition temperature in around 130 °C [12]. However, this weight loss is not

seen in the TGA curves of the Zn dust milled for longer time intervals such as 48 and 72 h, respectively as seen in Fig. 4c. When the milling time increases, due to the high milling impact energy, conversion of these hydroxides to more stable oxides readily takes place as per the reactions:

$$Zn(s) + 2H_2O(l) \rightarrow Zn(OH)_2(s) + H_2(g) \quad (4)$$

$$Zn(OH)_2(s) \rightarrow ZnO(s) + H_2O(l) \quad (5)$$

With further increase in temperature, oxidation of the Zn dust starts at around 400 °C causing a steep rise in the TGA curve. It is evident from the TGA curves; a gradual shift in the oxidation onset temperature with an increase in the milling time. From Fig. 4c, as the milling time is increased from 24 h to 48 h, the onset oxidation temperature drops by 35 °C from 471 °C to 436 °C. The TGA results indicate a further decrease of 35 °C when the milling time was raised from 48 to 72 h making the final oxidation onset temperature as 401 °C. Thus, the TG analysis clearly confirm a reduction of 98 °C in the oxidation onset temperature for milled Zn dust (72 h milled) compared to the un-milled raw Zn dust (Inset TGA curves in Fig. 4c). This effect in the onset oxidation temperature can be attributed to the increase in the specific surface area of the zinc dust due to particle size reduction during milling. Apart from the size effect, the formation of the atomic level ZnO surface seed-layer with milling also accelerated the reaction kinetics.

In fact, the seed particles slowly disperse in aqueous medium and in the absence of any surfactants, they tend to form primary ZnO seed-clusters and agglomerates. The particle size distribution analysis (DLS) of the seed suspension obtained at different milling time is presented in Fig. 5a. The pH of the milled medium was measured to be in the range 8.7–9.15 at the time when the measurement was taken. After 24 h of milling, the particle size analysis of ZnO seed-clusters in the suspension showed an average size of about 537 nm which was decreased to 217 nm when the milling time was increased from 24 to 72 h. The crystallite size of the seed particles from the milled dispersion was measured using Debye–Scherrer relation, these values also showed a similar trend. The crystallite size of the ZnO seeds formed decreased from 52.78 nm for 24 h milled samples to 42.22 nm for 48 h milled samples and further to 35.18 nm for 72 h milled.

The SEM and TEM images of the ZnO seeds formed after 72 h milling is shown in Fig. 5b and the inset in Fig. 5b. The clusters size of the seeds formed were measured to be ~135 nm. Thus the UV, XRD, TGA, TEM and DLS analyses confirmed the germination of nano sized ZnO seeds with the milling operation, which in effect favors the thermal oxidation of Zn dust into nanocrystalline ZnO at low temperatures without the aid of any catalysts.

3.2. Conventional (CTO) and microwave assisted (MW) thermal oxidation of Zn dust

After mechanical activation by milling, the oxidation of the modified zinc was conducted in both conventional and microwave conditions at well-above its on-set oxidation temperature. In the CTO route the zinc dust milled for 72 h was oxidized at 750 °C/7 h. This condition was found to be optimal for complete oxidation of Zn dust to nano ZnO. Anisotropic growth of ZnO was observed in this technique due to the slow heating and variation

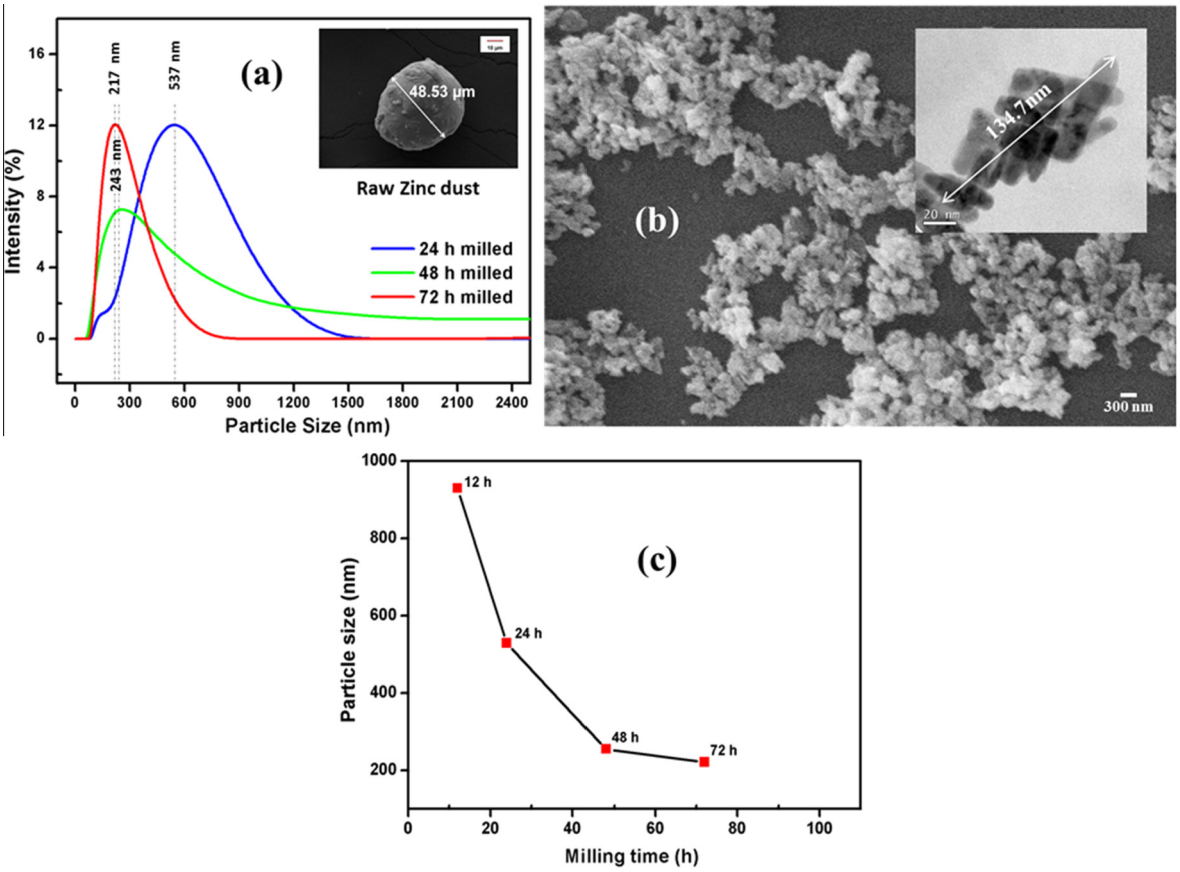

Fig. 5. (a) Size distribution (DLS) of ZnO seeds formed during milling for different time periods, SEM image of an unmilled raw dust particle having an average particle size value of 48.53 µm (Inset). (b) SEM image of ZnO seeds formed during milling after 72 h. (Inset, TEM of the ZnO seeds formed after 72 h milling). (c) Influence of milling time on ZnO seed cluster size (nm) measured by DLS.

in the oxygen concentration at the different regions of the muffle furnace. In the microwave route, the Zn dust milled for 72 h was irradiated for 15 min at the maximum power of 600 W. Here the direct transfer of electromagnetic energy to thermal energy causes rapid and uniform volumetric heating of the milled Zn and thus reducing the reaction time. The ZnO powders synthesized were characterized to compare and validate the two routes *viz* the Conventional Thermal Oxidation (CTO) and Microwave assisted Oxidation (MW).

3.3. Zn dust derived nano ZnO

Fig. 6 shows the XRD pattern of the Zn dusts after the thermal oxidation. Out of the several oxidation constraints tried (as shown in Table 2), complete oxidation of the Zn dust was achieved only in few cases. The XRD analysis conducted on randomly selected samples showed immature peaks of ZnO indicating the incompleteness in the oxidation process (Fig. 6a). In addition; the presence of certain contamination peaks also validates the incomplete oxidation. The phase analysis of the completely oxidized Zn dust by both the CTO (750 °C/7 h) and MW (600 W/10 min and 600 W/15 min) routes are shown in Fig. 6b. The XRD spectra of these samples confirmed the presence of phase pure hexagonal wurtzite ZnO in both the routes. All the crystalline peaks are matching well with the JCPDS file no: 36-1451. There are no peaks representing any sort of characteristic impurity phases, indicating a complete thermal conversion of Zn dust to nano crystalline ZnO.

It is noteworthy that in MW route, the oxidation is completed within 15 min showing the competitiveness of the technique. Even though, such rapid heating occurs in microwave fields, the crystalline quality of the end product, nano ZnO is not affected which is confirmed from the obtained lattice parameter values. ZnO has typical lattice parameter values, $a = 3.24$ Å and $c = 5.21$ Å, respectively [44]. Table 3 shows the lattice parameter values of the nano ZnO processed *via* MW and CTO routes. Interestingly, these values of ZnO derived by both techniques are near to the standard values revealing the processing advantage of the techniques. The lattice parameter values a and c confirms, the Zn dust derived nano ZnO is of wurtzite structure having hexagonal unit cells with the ratio $c/a = 1.633$ belonging to the space group C_{6v}^4 in the Schoenflies notation and $P6_3mc$ in the Hermann–Mauguin notation [45]. The XRD analysis further confirms that the increase in microwave exposure improves the crystallinity of the nano ZnO compared to conventional oxidation route.

Table 3
Lattice constants a, b, and c corresponding to the (101) crystal plane for ZnO synthesized through conventional (CTO) and microwave (MW) routes.

Samples	Processing conditions	Lattice parameter $a = b$ (Å)	Lattice parameter c (Å)
a	Microwave assisted oxidation (600 W/15 min)	3.21	5.24
b	Microwave assisted oxidation (600 W/10 min)	3.24	5.29
c	Conventional thermal oxidation (750 °C/7 h)	3.23	5.27

a, b and c are the samples presented in the Fig. 6(b).

3.3.1. Morphological features of nano ZnO

Fig. 7 shows the SEM and TEM microstructures of nano ZnO obtained from CTO and MW techniques. The CTO route produced dense irregularly shaped, agglomerated ZnO nanoparticles (Fig. 7a). However, the TEM image (Fig. 7b) confirms the formation of rod shaped crystallites having length ~100 nm and diameter of around 10 nm. On the other hand, SEM analysis (Fig. 7d) of the ZnO prepared *via* MW route seems to show nano-rod morphology where the length varies in micrometer range and the diameter in sub-micron scale. The TEM images (Fig. 7e) also confirms the perfect ZnO micro-rods having diameter of approximately 200 nm and length about 5–6 μm obtained through MW route. This drastic variation in the morphology of microwave oxidized ZnO can be attributed to the seed-assisted nucleation and growth. When compared to the conventional technique, the homogeneous reversible temperature gradients and rapid heat build-up in microwave assisted heating cause such an excessive, directionally uniform growth of the ZnO rods in MW route.

The selected area electron diffraction (SAED) patterns clearly shows the polycrystalline and mono-crystalline characters of the conventionally and microwave synthesized samples respectively

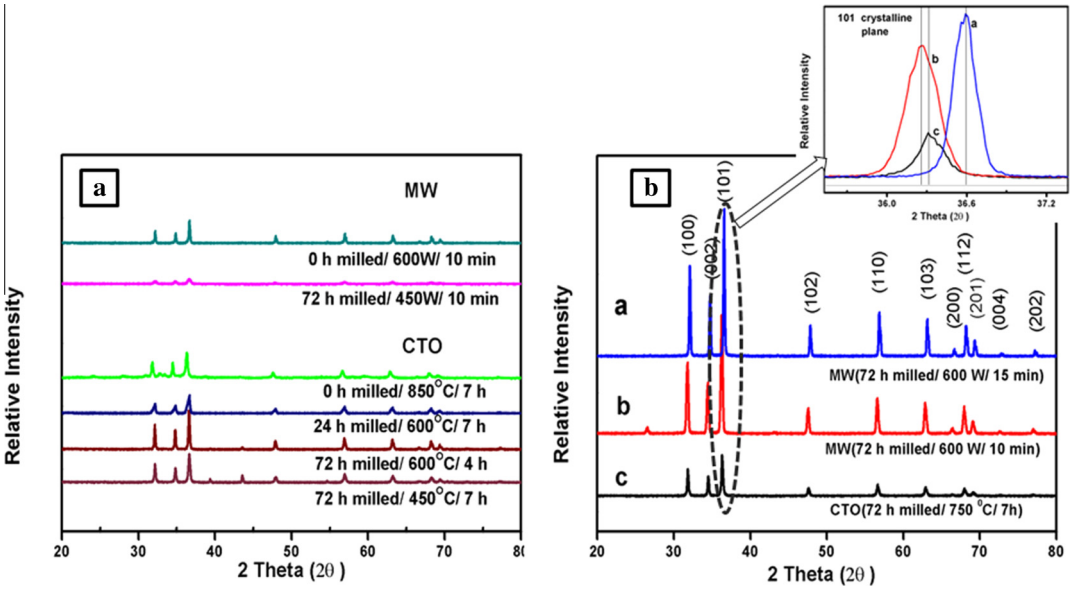

Fig. 6. (a) XRD patterns of randomly selected constraints from Table 2. (b) XRD patterns of the ZnO synthesized using the finally optimized and fixed CTO and MW routes (the (101) crystalline plane is highlighted).

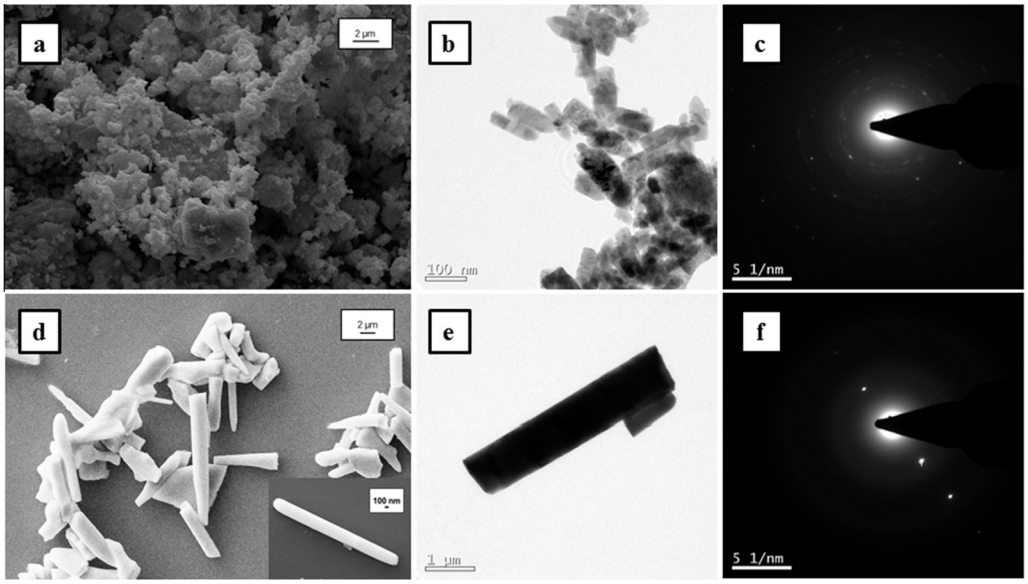

Fig. 7. SEM and TEM images and SAED patterns of ZnO synthesized *via* CTO route (a–c) and MW route (d–f). (Inset in (d) shows the SEM image of a single nanorod obtained by MW route).

(Fig. 7c and Fig. 7f). The microwave energy acting on the bulk Zn reduce the surface energy causing unidirectional growth [46], resulting in the formation of highly crystalline nano-structures, like nano rods in this case. The optimized routes and the brief morphological and dimensional statistics of the final ZnO formed is given in Table 4.

4. NIR reflective and anti-corrosive studies of nano-ZnO functional coatings

The applicability of Zn dust derived ZnO nanoparticles for obtaining multifunctional coatings was tested. Blends were prepared with CNSL resin as the matrix and Zn derived nano ZnO powder as the filler. The coatings were examined optically for microstructural defects and the results are presented in Fig. 8a–f. The optical images of the neat CNSL coating was compared with the CNSL base loaded with different volume percentages (5% and 10%) of the nano ZnO synthesized *via* CTO and MW routes. Its is evident that in the case of pure CNSL coatings, there are many deep level drying-cracks and possible detachment of the layer from the glass surface/substrate. However, the addition of nano ZnO into CNSL base has clearly reduced this problem and has formed uniform coatings. It is also observed that CNSL base loaded with 10 vol% of nano ZnO synthesized through MW route, ZnO (MW) 10 (Fig. 8f) is forming the best in class coating. This can be attributed to the typical morphology of the ZnO which roots an excellent knitting effect forming good and crack free coatings, when compared to the coatings of pure CNSL and CNSL with ZnO prepared through conventional route, with the same percentage loading, ZnO (CTO) 10 (Fig. 8e). Thus the loading percentage of synthesized ZnO for coatings was fixed at 10 vol% for further application studies. The XRD analysis (Fig. 8g) of the coatings developed confirmed the amorphous nature of CNSL resin. When this CNSL was loaded with ZnO, the coatings showed the characteristic crystalline peaks of ZnO at their respective positions. It is also clearly apparent that the XRD peaks are more prominent in the case of coatings having ZnO (MW) 10 compared to those with ZnO (CTO) 10. This can be attributed to the better crystalline purity of ZnO synthesized through the MW route [47].

The water contact angle measured for the CNSL + ZnO coatings was compared with the uncoated surface and is shown in Fig. 8h. Overall the coatings found to have significant hydrophobic surface character. The contact angle value obtained was 34° for uncoated glass, showing the hydrophilic nature of the glass surface. With pure CNSL coatings the contact angle is increased to 91°, showing the significant hydrophobic character imparted due to the presence of cardonol. Chemically unmodified cardonol is known to have inherently long-hydrophobic hydrocarbon chains with a slightly polar phenolic ring, and hence showing good water repellent character [48]. As seen in the optical images (Fig. 8a and b), crack growth in pure CNSL coatings makes the surface more rough, infact reducing its characteristic water repellent nature [49]. However, this effect seems to be minimal as the coating still maintains its hydrophobicity.

With the inclusion of nano ZnO into the CNSL matrix, the contact angle values marginally dropped to 86° and 78° for CTO and MW derived ZnO, respectively. These nanostructured ZnO, in the absence of any surface active agents such as silane is known to have high hydrophilic nature [4]. Also, there is a reduction in the number of reactive surface hydroxyl groups in the CNSL base with filler addition [48]. These two factors together contribute to the reduction in the contact angle values. At the same time, due to the reduced crack generation tendency of the coatings, the surface

Table 4
Brief statistics of the final ZnO through both the routes (CTO and MW).

Samples	Milling time/oxidation condition	Morphology	DLS (nm)	D_{XRD} (nm)	D_{TEM} (nm)		Aspect ratio
CTO	72 h/750 °C/7 h	Assorted	~404	81.96	100–150		–
MW	72 h/600 W/15 min	1D nanorods	–	55.56	*l* ~5120	*d* ~260	~19.6

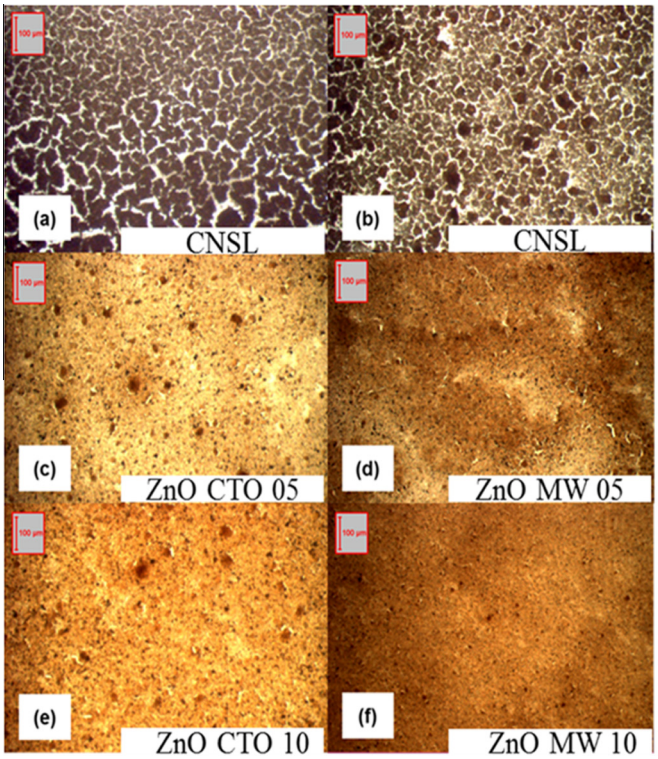

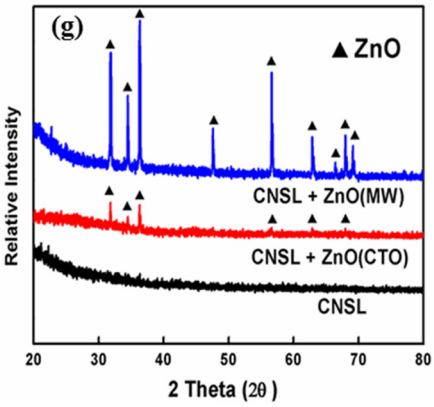

(h)	Contact Angle
Glass (Uncoated)	34± 4.6°
Glass + CNSL	91± 0.61°
Glass + CNSL +ZnO (CTO)	86± 8.6°
Glass + CNSL +ZnO (MW)	78± 6.9°

Fig. 8. Optical images of coatings made over glass. (a and b) Pure CNSL. (c and d) CNSL with 5 vol% ZnO synthesized *via* CTO and MW routes respectively. (e and f) CNSL with 10 vol% ZnO synthesized *via* CTO and MW routes respectively. (g) XRD patterns of the coatings, pure CNSL and CNSL loaded with 10% (by vol) of ZnO. (h) Contact Angle measured for uncoated glass, CNSL and CNSL + ZnO 10% (by vol) coated glass surfaces.

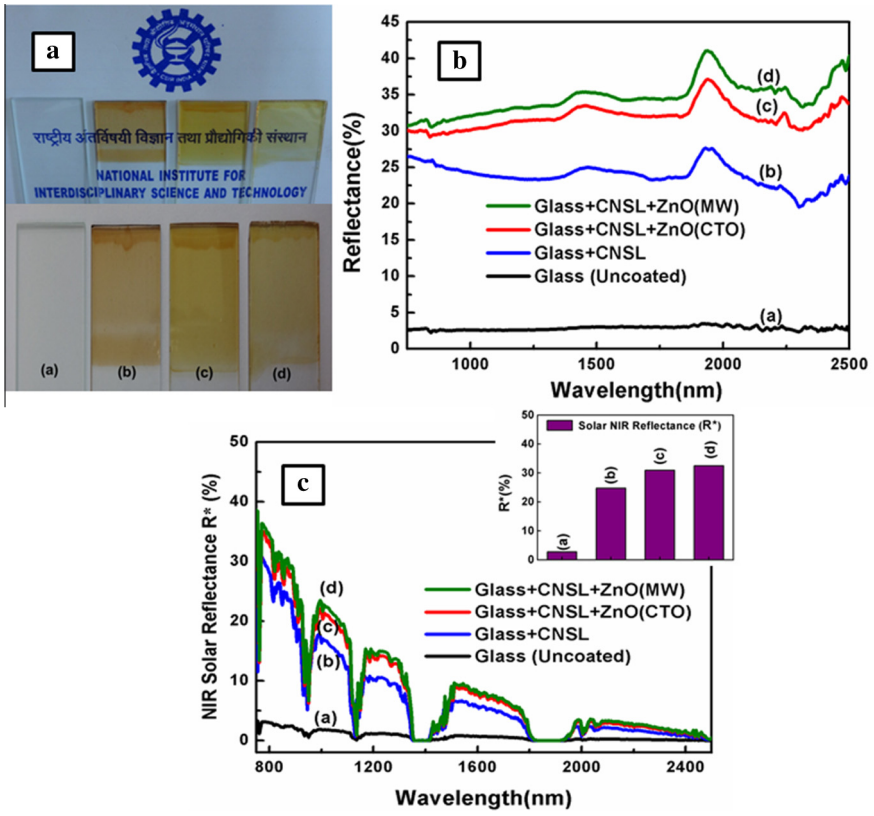

Fig. 9. (a) CNSL based transparent coatings made on glass. (b) NIR reflectance spectra of different coatings made, (c) NIR solar reflectance (R^*) of different coatings made on glass, with the bar chart showing R^* value of different coatings.

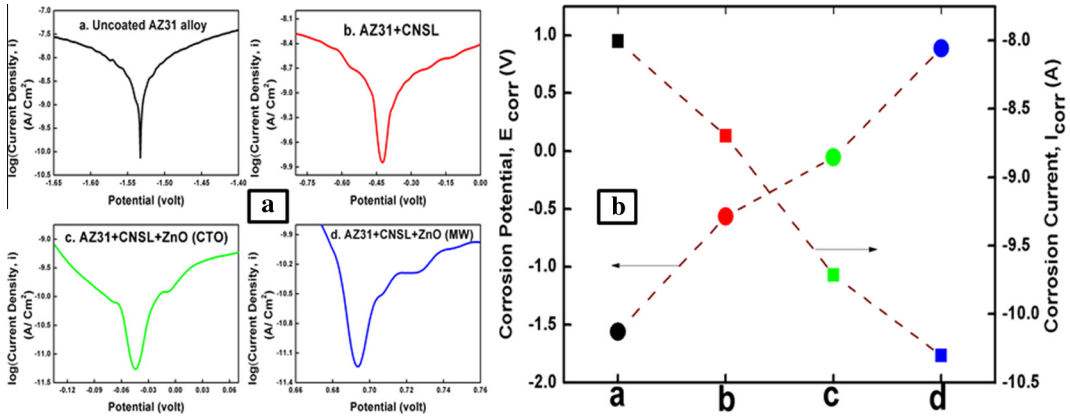

Fig. 10. (a) Tafel Plots of the different coatings made over AZ31 alloy. (b) Variation of the Corrosion Potential (E_{corr}) and Corrosion Current (I_{corr}) for the different coatings.

roughness decreases which results in an increase in the contact angle value. However, inspite of all these factors affecting the contact angle value, the overall change in the value is not so significant, and the coatings still maintains its water-repelling character.

4.1. IR shielding characteristics

Fig. 9 shows the NIR reflectance of the coatings developed. From Fig. 9a it is evident that the coatings developed have good optical transparency with the possibility for obtaining brown tinted transparent functional coatings. The NIR reflectance efficiency of these CNSL based transparent ZnO coatings were measured and compared with pure CNSL coatings and uncoated glass surfaces. Fig. 9b shows the NIR reflectance properties of CNSL coatings prepared with and without addition of nano ZnO. It is evident that bare glass have low NIR reflectance value (below 3%) but when it was applied with CNSL coatings, it attained considerable NIR reflecting property.

The CNSL coatings containing nano ZnO showed nearly 35% improvement in NIR reflectance. It also has to be noted that, among the MW and CTO derived nano ZnO, the coatings made with MW derived nano ZnO has better NIR reflecting property. The Solar NIR reflectance is also enhanced (Fig. 9c) with the incorporation of the as-synthesized ZnO in the organic base.

4.2. Corrosion resistance study

The electro chemical corrosion resistance property of the nano ZnO dispersed CNSL coatings was evaluated using AZ31 Mg alloy which is prone to corrosion. Fig. 10a shows the respective Tafel plots of the coatings prepared. The Mg alloy coated with both pure CNSL and nano ZnO dispersed CNSL showed remarkably better performance than the uncoated surface. It can be seen that there is a shift in the corrosion potential (E_{corr}) from the negative to the positive values; showing the corrosion resistance efficiency of the ZnO/CNSL coatings over the bare alloy. The E_{corr} value increased from −1.56 V for bare alloy to a value of 0.887 V for the surface coatings prepared with CNSL + ZnO(MW) 10. The cardanol due to its phenolic character and the long alkly side chain has corrosion deterring ability [50]. Moreover, the rod shaped nano ZnO particles synthesized *via* MW route effectively by-pass the current conduction path due to a the better knitting of the particles when compared to CTO synthesized ZnO. The decrease in the corrosion current (I_{corr}) value (as shown in Fig. 10b) also shows the corrosion resistance imparted by ZnO/CNSL coatings. The corrosion current value obtained was −8.004 A for the uncoated alloy surface, which gradually decreased to −10.3 A for CNSL + ZnO(MW) 10 coated surface. Thus it can be inferred that, ZnO dispersed CNSL based coatings forms an effective protective outer crust for similar corrosion prone alloys.

5. Conclusions

Nano ZnO synthesis through microwave assisted thermal oxidation was optimized and the product was validated for special functional coatings. Mechanically modified Zn dust showed the growth of ZnO seed nuclei in 48 h of milling and the milled Zn dust undergoes comparatively early oxidation. A complete conversion of Zn dust into nano ZnO is accomplished within 15 min reaction time, under microwave heating. Further in the oxidation part, it can be seen that the microwave assisted oxidation shows significant advancement in the particle morphology. Thus, single phase, mono-crystalline nano ZnO rods can be successfully synthesized by the microwave assisted oxidation (600 W/15 min) of mechanically modified (ball-milled for 72 h) raw Zn dust under the optimized conditions. The application studies conducted with the synthesized ZnO also turned out to be positive. A functional paint coating prepared by dispersing nano ZnO in CNSL resin showed significant improvement in the NIR reflectance. A measured NIR Reflectance value of <3% for bare glass is enhanced to 24% for CNSL + ZnO (CTO) 10 coatings which was further improved to 33% for CNSL + ZnO (MW) 10. The corrosion studies conducted through an electrochemical route also showed remarkable improvement in the corrosion resistance imparted by these coatings on the bare Mg alloy. With the coating of CNSL + ZnO (MW) 10, about 156% improvement in the corrosion resistance compared to uncoated surface was observed. Thus in nutshell, the whole work focuses on developing a new, cost effective, catalyst-free technique for synthesizing nano grade ZnO from raw Zn dust that will transpire into various special multipurpose coating applications.

Acknowledgements

The authors thank The Director, CSIR-NIIST, Thiruvananthapuram for providing the lab facility for the work. The author sincerely acknowledges M/s Binani Zinc Pvt. Ltd. for the financial support and the raw Zinc dust which was used in this work. The authors also thank Mr. Kiran Mohan for TEM analysis, Ms. Sheethu Jose and Ms. Anaswara Jayaprakash for the NIR measurements, Ms. Jerin K. Pancrecious and Ms. Remya Rajan for the corrosion studies.

References

[1] X. Ma, M.R. Zachariah, Oxidation anisotropy and size-dependent reaction kinetics of zinc nanocrystals, J. Phys. Chem. C 113 (2009) 14644–14650.
[2] M. Xu, D.G. Ivey, Z. Xie, W. Qu, Rechargeable Zn-air batteries: progress in electrolyte development and cell configuration advancement, J. Power Sources 283 (2015) 358–371.
[3] N. Arianpouya, M. Shishesaz, M. Arianpouya, M. Nematollahi, Evaluation of synergistic effect of nanozinc/nanoclay additives on the corrosion performance of zinc-rich polyurethane nanocomposite coatings using electrochemical properties and salt spray testing, Surf. Coat. Technol. 216 (2013) 199–206.
[4] A. Moezzi, A.M. McDonagh, M.B. Cortie, Zinc oxide particles: synthesis, properties and applications, Chem. Eng. J. 185–186 (2012) 1–22.
[5] A. Kolodziejczak-Radzimska, T. Jesionowski, *Zinc* oxide – from synthesis to application: a review, Materials 7 (2014) 2833–2881.
[6] R.N. Jagtap, P.P. Patil, S.Z. Hassan, Effect of zinc oxide in combating corrosion in zinc-rich primer, Prog. Org. Coat. 63 (2008) 389–394.
[7] R. Schmid-Fetzer, B. Hallstedt, Is zinc HCP_ZN or HCP_A3?, Calphad 37 (2012) 34–36
[8] Y. Alemdag, M. Beder, Microstructural, mechanical and tribological properties of Al–7Si–(0–5) Zn alloys, Mater. Des. 63 (2014) 159–167.
[9] N.M. Ahmed, H.T.M. Abdel-Fatah, E.A. Youssef, Corrosion studies on tailored Zn Co aluminate/kaolin core–shell pigments in alkyd based paints, Prog. Org. Coat. 73 (2012) 76–87.
[10] M. Echeverria, C.M. Abreu, F.J. Deive, M.A. Sanroman, A. Rodriguez, Ionic liquids improve the anticorrosion performance of Zn-rich coatings, RSC Adv. 4 (2014) 59587–59593.
[11] Wendusu, T. Honda, T. Masui, N. Imanaka, Novel environmentally friendly (Bi, Ca, Zn, La) VO_4 inorganic yellow pigments, RSC Adv. 3 (2013) 24941–24945.
[12] X. Ma, M.R. Zachariah, Size-resolved kinetics of Zn nanocrystal hydrolysis for hydrogen generation, Int. J. Hydrogen Energy 35 (2010) 2268–2277.
[13] L. Xiao, S.-Y. Wu, Y.-R. Li, Advances in solar hydrogen production *via* two-step water-splitting thermochemical cycles based on metal redox reactions, Renew. Energy 41 (2012) 1–12.
[14] F. Fang, D.X. Zhao, J.Y. Zhang, D.Z. Shen, Y.M. Lu, X.W. Fan, B.H. Li, X.H. Wang, The influence of growth temperature on ZnO nanowires, Mater. Lett. 62 (2008) 1092–1095.
[15] Y. Zhang, S. Zhuang, X. Xu, J. Hu, Transparent and UV-shielding ZnO @ PMMA nano-composite films, Opt. Mater. (2013), http://dx.doi.org/10.1016/j.optmat.2013.08.021.
[16] S. Soumya, A. Peer Mohamed, Lucy Paul, M. Kiran, S. Ananthakumar, Near IR reflectance characteristics of PMMA/ZnO nano composites for solar thermal control interface films, Sol. Energy Mater. Sol. Cells 125 (2014) 102–112.
[17] I. Banerjee, R.C. Pangule, R.S. Kane, Antifouling coatings: recent developments in the design of surfaces that prevent fouling by proteins, bacteria and marine organisms, Adv. Mater. 23 (2011) 690–718.
[18] R. Wang, H. Tan, Z. Zhao, G. Zhang, L. Song, W. Dong, Z. Sun, Stable ZnO@TiO_2 core/shell nanorod arrays with exposed high energy facets for self-cleaning coatings with anti-reflective properties, J. Mater. Chem. A 2 (2014) 7313–7318.
[19] L. Wang, M. Wen, M. Zhang, L. Jiang, Y. Zheng, Ice-phobic gummed tape with nano-cones on microspheres, J. Mater. Chem. A 2 (2014) 3312–3316.
[20] Z.L. Wang, Zinc oxide nanostructures: growth, properties and applications, J. Phys.: Condens. Matter 16 (2004) 829–858.
[21] A.B. Djurisic, X. Chen, Y.H. Leung, A.M.C. Ng, ZnO nanostructures: growth, properties and applications, J. Mater. Chem. 22 (2012) 6526–6535.
[22] Y. Zhang, L. Wang, X. Liu, Y. Yan, C. Chen, J. Zhu, Synthesis of nano/micro zinc oxide rods and arrays by thermal evaporation approach on cylindrical shape substrate, J. Phys. Chem. B 109 (2005) 13091–13093.
[23] C.X. Zhao, Y.F. Li, J. Zhou, L.Y. Li, S.Z. Deng, N.S. Xu, Jun Chen, Large-scale synthesis of bicrystalline ZnO nanowire arrays by thermal oxidation of zinc film: growth mechanism and high-performance field emission, Cryst. Growth Des. 13 (2013) 2897–2905.
[24] S.A. Kamaruddin, K.-Y. Chan, H.-K. Yow, M.Z. Sahdan, H. Saim, D. Knipp, Zinc oxide films prepared by sol–gel spin coating technique, Appl. Phys. A 104 (2011) 263–268.
[25] N.J. Nicholas, G.V. Franks, W.A. Ducker, The mechanism for hydrothermal growth of zinc oxide, CrystEngComm 14 (2012) 1232–1240.
[26] J. Lu, K.M. Ng, Efficient, one-step mechanochemical process for the synthesis of ZnO nanoparticles, Ind. Eng. Chem. Res. 47 (2008) 1095–1101.
[27] E. Kandjani, M.F. Tabriz, B. Pourabbas, Sonochemical synthesis of ZnO nanoparticles: the effect of temperature and sonication power, Mater. Res. Bull. 43 (2008) 645–654.
[28] A.V. Maciel, W. da Nova Mussel, V.M.D. Pasa, A novel synthesis of nanostructured ZnO *via* thermal oxidation of Zn nanowires obtained by green route, Mater. Sci. Appl. 1 (2010) 279–284.
[29] L. Yuan, C. Wang, R. Cai, Y. Wang, G. Zhou, Temperature-dependent growth mechanism and microstructure of ZnO nanostructures grown from the thermal oxidation of zinc, J. Cryst. Growth 390 (2014) 101–108.
[30] Y.-J. Zhu, F. Chen, Microwave-assisted preparation of inorganic nanostructures in liquid phase, Chem. Rev. 114 (2014) 6462–6555.
[31] X. Zou, H. Fan, Y. Tian, M. Zhang, X. Yan, Microwave-assisted hydrothermal synthesis of Cu/Cu_2O hollow spheres with enhanced photocatalytic and gas sensing activities at room temperature, Dalton Trans. 44 (2015) 7811–7821.
[32] D.-S. Wu, C.-Y. Han, S.-Y. Wang, N.-L. Wu, I.A. Rusakova, Microwave-assisted solution synthesis of SnO nanocrystallites, Mater. Lett. 53 (2002) 155–159.
[33] X. Hu, J. Gong, L. Zhang, J.C. Yu, Continuous size tuning of monodisperse ZnO colloidal nanocrystal clusters by a microwave-polyol process and their application for humidity sensing, Adv. Mater. 20 (2008) 4845–4850.
[34] T. Krishnakumar, R. Jayaprakash, Nicola Pinna, V.N. Singh, B.R. Mehta, A.R. Phani, Microwave-assisted synthesis and characterization of flower shaped zinc oxide nanostructures, Mater. Lett. 63 (2009) 242–245.
[35] A. Phuruangrat, T. Thongtem, S. Thongtem, Microwave-assisted synthesis of ZnO nanostructure flowers, Mater. Lett. 63 (2009) 1224–1226.
[36] C.F. Burmeister, A. Kwade, Process engineering with planetary ball mills, Chem. Soc. Rev. 42 (2013) 7660–7667.
[37] V. Sepelak, S. Begin-Colin, G. Le Caer, Transformations in oxides induced by high-energy ball-milling, Dalton Trans. 41 (2012) 11927–11948.
[38] Y. Fan, H. Yang, M. Li, G. Zou, Evaluation of the microwave absorption property of flake graphite, Mater. Chem. Phys. 115 (2009) 696–698.
[39] M. Naebe, J. Wang, A. Amini, H. Khayyam, N. Hameed, L.H. Li, Y. Chen, B. Fox, Mechanical property and structure of covalent functionalised graphene/epoxy nanocomposites, Sci. Rep. 4 (4375) (2014) 1–7.
[40] K.B. Babitha, V. Linsha, S. Anas, A. Peer Mohamed, M. Kiran, S. Ananthakumar, Microwave assisted aqueous synthesis of organosilane treated mesoporous Si@ZnO nano architectures as dual-functional, photocatalysts, J. Environ Chem. Eng. (2014), http://dx.doi.org/10.1016/j.jece.2014.12.010.
[41] S. Jose, A. Prakash, S. Laha, S. Natarajan, M.L. Reddy, Green colored nano-pigments derived from Y_2BaCuO_5: NIR reflective coatings, Dyes Pigm. 107 (2014) 118–126.
[42] T. Xing, J. Sunarso, W. Yang, Y. Yin, A.M. Glushenkov, L.H. Li, P.C. Howlett, Y. Chen, Ball milling: a green mechanochemical approach for synthesis of nitrogen doped carbon nanoparticles, Nanoscale 5 (2013) 7970–7976.
[43] G.M. Hughes, G.E. Smith, P.E.J. Flewitt, A.G. Crocker, The brittle fracture of polycrystalline zinc, Proc. R. Soc. A 463 (2007) 2129–2151.
[44] R. Vinodkumar, K.J. Lethy, P.R. Arunkumar, R.R. Krishnan, N.V. Pillai, V.P.M. Pillai, Reji Philip, Effect of cadmium oxide incorporation on the microstructural and optical properties of pulsed laser deposited nanostructured zinc oxide thin films, Mater. Chem. Phys. 121 (2010) 406–413.
[45] H. Morkoc, U. Ozgur, Zinc Oxide: Fundamentals, Materials and Device Technology, Wiley-VCH Verlag GmbH and Co. KGaA, Weinheim, 2009.
[46] L. Zhang, Y.J. Zhu, ZnO micro- and nano-structures: microwave-assisted solvothermal synthesis, morphology control and photocatalytic properties, Appl. Phys. A 97 (2009) 847–852.
[47] H-qin Liang, L-zhan Pan, Z-jun Liu, Synthesis and photoluminescence properties of ZnO nanowires and nanorods by thermal oxidation of Zn precursors, Mater. Lett. 62 (2008) 1797–1800.
[48] V.S. Balachandran, S.R. Jadhav, P.K. Vemula, G. John, Recent advances in cardanol chemistry in a nutshell: from a nut to nanomaterials, Chem. Soc. Rev. 42 (2013) 427–438.
[49] M.-H. Zhao, X.-P. Chen, Q. Wang, Wetting failure of hydrophilic surfaces promoted by surface roughness, Sci. Rep. 4 (5376) (2014) 1–5.
[50] D. Balgude, A.S. Sabnis, CNSL: an environment friendly alternative for the modern coating industry, J. Coat. Technol. Res. 11 (2014) 169–183.